Click Here for Full Article

Effects of mass waste events on thrust wedges: Analogue experiments and application to the Makran accretionary wedge

Jeroen Smit,[1,2] Jean-Pierre Burg,[1] Asghar Dolati,[1,3] and Dimitrios Sokoutis[4]

[1] Olistostromes cover large portions of active thrust wedges like Makran, Gulf of Cadiz, and offshore Borneo. Olistostrome emplacement by submarine mass flow represents an instantaneous and massive mass redistribution that may influence thrust wedge mechanics. Different scenarios are experimentally tested. They show that the postolistostrome wedge development depends on the thickness and extent of the added load. These results are discussed after the example of the Iranian Makran wedge, situated between the Arabian and Eurasian plates. Mass redistribution caused by a late Miocene mass flow may explain a change in deformation style from intense folding and thrusting to gentle folding and eventually a jump of thrust imbrication toward the frontal offshore part of this active accretionary wedge. **Citation:** Smit, J., J.-P. Burg, A. Dolati, and D. Sokoutis (2010), Effects of mass waste events on thrust wedges: Analogue experiments and application to the Makran accretionary wedge, *Tectonics*, *29*, TC3003, doi:10.1029/2009TC002526.

1. Introduction

1.1. Olistostromes and Thrust Wedges

[2] Olistostromes cover large portions of active thrust wedges like the Sunda Arc [*Moore et al.*, 1976], the Gibraltar Accretionary Wedge, Gulf of Cadiz [*Medialdea et al.*, 2004], and offshore Borneo [*Gee et al.*, 2007; *Morley*, 2007]. Fossil equivalents can be studied in outcrop in the Apennines [*Pini*, 1999; *Bonini*, 2006; *Lucente and Pini*, 2008], the Andes [*Callot et al.*, 2008], and Makran [*McCall and Kidd*, 1982; *Burg et al.*, 2008]. The Makran accretionary wedge (Figure 1) offers exceptionally clear exposures where the size, the stratigraphy, the morphology and the primary structures of the wedge can be studied without conjecture. A huge olistostrome is intercalated in the upper Miocene deposits (Figure 2) [*Burg et al.*, 2008]. It has been interpreted as a gigantic, catastrophic mass flow on the growing wedge. The consequences of such a sudden and considerable mass redistribution on the wedge evolution set the questions we aim to answer in this work.

[3] The geometry of a thrust wedge and internal thickening versus frontal accretion depend on the equilibrium between internal wedge strength and resistance along its base, provided its bulk rheology is that of a Coulomb material [e.g., *Chapple*, 1978; *Davis et al.*, 1983]. Regular, noncatastrophic surface processes lengthen the life span of individual thrust faults and therefore delay the forward development of new thrusts and the subsequent frontward growth of the thrust wedge [e.g., *Storti and McClay*, 1995; *Persson et al.*, 2004; *Konstantinovskaia and Malavieille*, 2005; *Bonnet et al.*, 2007]. The influence of erosion and sedimentation versus tectonic processes on deformation and geometry of thrust wedges has been the subject of many studies. However, studies of natural examples are strongly hindered by the different temporal and spatial scales of surface versus tectonic processes.

[4] The downslope displacement over large distances of huge rock masses may be sufficient to introduce a mechanical imbalance and force a reequilibration and changes in the wedge evolution [e.g., *Morley*, 2007; *Burg et al.*, 2008]. Studying the mechanical consequences of extreme events like large mass flows contributes to the understanding of the relative importance of surface versus internal deformation processes in thrust wedges. We use the example of the Iranian Makran and the results from new analog experiments to discuss the effects of olistostrome emplacement on thrust wedge mechanics and evolution.

1.2. Makran

[5] The Makran accretionary wedge, between the Arabian and Eurasian plates, grows seaward by frontal accretion and underplating of trench-fill sediments since early Miocene (Burdigalian), at least, at a present rate of about 2 cm/yr [e.g., *Bayer et al.*, 2006; *Vigny et al.*, 2006].

[6] The >300 km width of the Makran wedge and a low cross-sectional taper of ~3° suggest low basal friction and, most probably, the presence of one or more weak décollements (Figure 2b). Active mud volcanoes [e.g., *Harrison*, 1944; *Snead*, 1964; *von Rad et al.*, 2000; *Delisle et al.*, 2002] may indicate that such décollements take advantage of overpressured shales.

[7] The Makran wedge includes a giant olistostrome (Figure 3) containing blocks of ophiolites and oceanic sediments derived from the tectonic "mélange" to the north [*McCall and Kidd*, 1982] and reworked pieces of the turbidites on which it rests with an erosional unconformity [*Burg et al.*, 2008]. In the south, where the substrate is made of Middle Miocene slope deposits, the basal contact is

---

[1]Geological Institute, ETH and University Zurich, Zurich, Switzerland.
[2]Now at ISTeP, UMR 7193, Université Pierre and Marie Curie, Paris, France.
[3]Geological Survey of Iran, Tehran, Iran.
[4]Netherlands Research Centre for Integrated Solid Earth Sciences, Faculty of Earth and Life Sciences, Vrije Universiteit, Amsterdam, Netherlands.
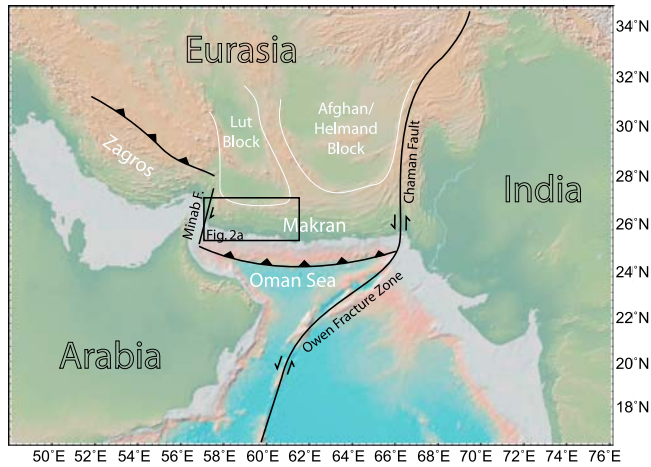
Figure 1. Tectonic setting of the Makran subduction zone on a digital elevation model of combined land topography (SRTM) and marine bathymetry [*Smith and Sandwell*, 1997], generated with the GeoMapApp interface (http://www.geomapapp.com).

nearly parallel to the sediment layers with apparently limited or no erosion. The size and internal structure of this olistostrome make it a fossil equivalent of the large debris flows found along continental margins.

[8] At the time of olistostrome emplacement, during the Tortonian (around 10 Ma), the well-developed thrust wedge measured at least 150 km from back to front and presumably looked like the present-day offshore Makran (Figure 2b); a frontward propagating thrust wedge with a weak basal ductile décollement level and low cross-sectional taper, covered in its internal part by thick, prograding sequences of rapidly sedimented mudstone and sandstone beds (3–4 km since the Pleistocene) [*Harms et al.*, 1984]. In the case of the Tortonian Makran, these sediments mainly consisted of shale-dominated siliciclastics as indicated by the mudstone matrix of the younger olistostrome. Around 10 Ma, this unit collapsed during a catastrophic event. The olistostrome increased its size during downslope transportation by off scraping and entailing of unconsolidated sediments (Figure 4), before coming to rest where it is found today (Figure 2). Such off scraping is a common process. In the case of the Brunei event,
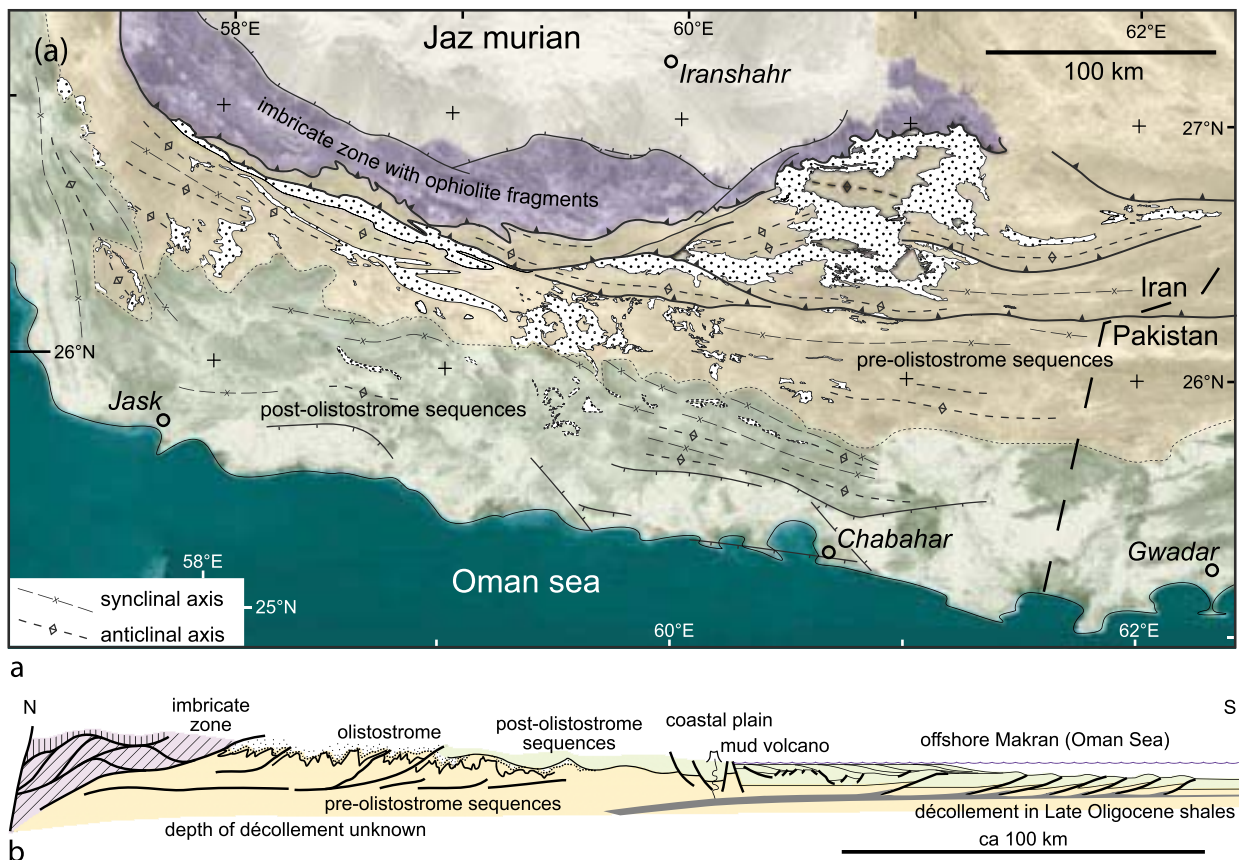

Figure 2. (a) Structural sketch map of the Iranian Makran with areal distribution of the Tortonian olistostrome (white areas, from *Burg et al.* [2008]). Fault symbols in hanging walls are according to international convention. (b) Synthetic section across the Makran accretionary complex (modified and extended from *Burg et al.* [2008]). The offshore wedge is compiled from data and interpretations from *Harms et al.* [1984], *Grando and McClay* [2007], and *Ellouz-Zimmermann et al.* [2007b]. The late Oligocene age of the offshore décollement is inferred from the age of planktonic foraminifera in the mud extruded in onshore mud volcanoes (S. Spezzaferri, personal communication, 2009).
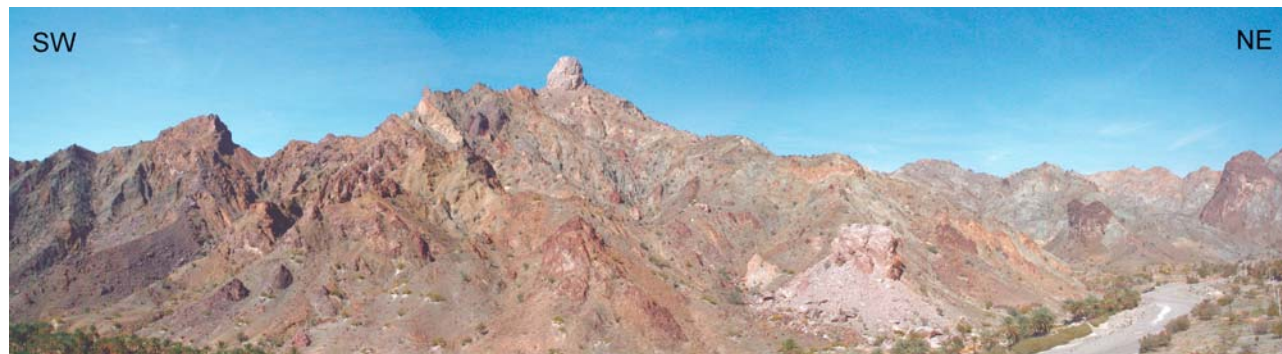
Figure 3. Panoramic view of the Tortonian olistostrome containing blocks of ophiolites and oceanic sediments derived from the tectonic "mélange" to the north [*McCall and Kidd*, 1982] and reworked pieces of the turbidites on which it rests with an erosional unconformity [*Burg et al.*, 2008]. Outcrop at 26°20.512′N; 26°18.503′E.

for instance, off-scraped sediments make up approximately 80% of the olistostrome [*Gee et al.*, 2007; *Morley*, 2007].

[9] The 10 Myr that have elapsed since olistostrome emplacement are short enough to preserve initial relationships but considered sufficient for mechanical reequilibration within the wedge. The Paleogene units of the northern Makran are characterized by large thrusts and strong internal deformation of thrust units expressed by tight folds and associated axial plane cleavage [*McCall*, 2002; *Burg et al.*, 2008]. Thrust activity in northern Makran started in the early Miocene and continued into the Quaternary, both in the Pakistani [*Ellouz-Zimmermann et al.*, 2007a] and Iranian (our personal observations, 2005–2009) parts. The olistostrome locally shows a weak cleavage but is much less intensely deformed than the older units it has unconformably covered. The dominantly Miocene and younger units of the Coastal Makran are deformed into large-wavelength–small-amplitude folds [*McCall*, 2002; *Burg et al.*, 2008]. Axial plane cleavage is generally absent as are large displacements along thrusts [*Burg et al.*, 2008]. Since the late Miocene/Pliocene the main deformation has shifted to the submarine, frontal Makran. Ongoing shortening is responsible for the reactivation of few thrusts in the onshore wedge [*Ellouz-Zimmermann et al.*, 2007a; J. Smit et al., personal observations, 2005–2009] but is mostly accommodated by frontal accretion above a midlevel décollement [e.g., *Harms et al.*, 1984; *Grando and McClay*, 2007; *Ellouz-Zimmermann et al.*, 2007b]. The sediments located below this décollement are underplated [*Platt et al.*, 1985] or transported into the mantle together with the subducting plate.

2. Analogue Modeling

2.1. Experimental Setup

[10] Experimental studies have addressed the link between noncatastrophic surface processes and deformation in
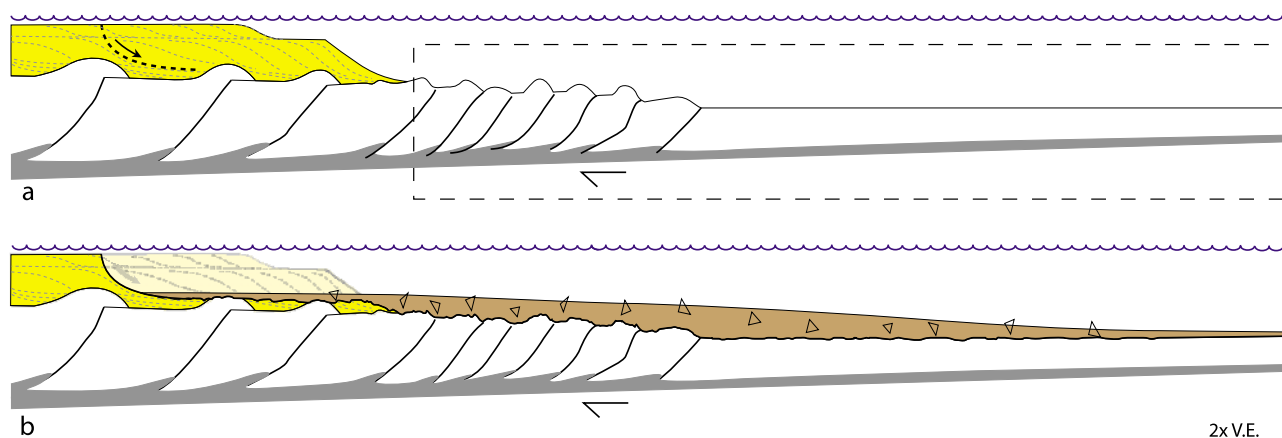

Figure 4. (a) Schematic profile of an accretionary wedge covered by a large sediment unit deposited on top of its internal part (geometry is roughly based on that of the present-day offshore Makran, Figure 2b). Dotted line indicates possible normal faults in this unit due to gravitational processes. The dashed rectangle indicates the wedge segment modeled in this study. (b) The wedge after olistostrome emplacement. Collapse of overthrust and sediment units creates the mass flow that covers the accretionary wedge far beyond the most frontal thrust.

Table 1. Model Parameters[a]

Model	Push/Pull	Load Size	Width (cm)	L_{DL} (cm)	Th_{DL} (cm)	Th_{sand} (cm)	V (cm/h)	x_1 (cm)	x_2 (cm)	x_T (cm)
1	push	L	40	100	0.7	1.8	3.0	7.5	5.0	12.5
2	push	M	40	100	0.7	1.3	3.0	18	2.1	20.1
3	push	S	40	100	0.7	1.3	3.0	12	5.5	17.5
4	pull	M	68	120	0.7	1.3	1.5	12.8	7.8	20.6

[a]Push/pull, the mode of shortening; by pushing the backstop or pulling a basal plastic sheet; load size, L, large; S, small; M, medium; width, width of experiment; L_{DL}, length of basal ductile layer; Th_{DL}, thickness of basal ductile layer; Th_{sand}, thickness of initial sand layer; V displacement rate; x_1, shortening during phase 1; x_2, shortening during phase 2; x_T, total amount of shortening.

compressional systems [e.g., *Storti and McClay*, 1995; *Mugnier et al.*, 1997; *Leturmy et al.*, 2000; *Barrier et al.*, 2002; *Persson et al.*, 2004; *Konstantinovskaia and Malavieille*, 2005; *Bonnet et al.*, 2007, 2008; *Graveleau and Dominguez*, 2008].

[11] The presented laboratory experiments were designed to investigate the influence of the instantaneous addition of a load, as represented by the Makran olistostrome, on the evolution of a thrust wedge. It is not the aim to reproduce a mass flow itself or the processes/mechanics involved in its emplacement. Experimental design is based on the following assumptions:

1. The thrust wedge is thin skinned, i.e., the basement is not involved in thrusting. Its rheology, excluding the décollement(s), is that of a Coulomb material, sand being a proper analog [*Hubbert*, 1937].

2. The wedge includes one or several weak and ductile décollements that facilitate forward propagation of the deformation front.

3. The rheology of the basal décollement is ductile, independent of the amount of overburden.

4. The wedge has a low surface angle after emplacement due to a low cohesion/viscosity of the olistostrome. The chaotic structure and mixing of different rock types, in particular that of the mudstone matrix, are indications for such a low cohesion/viscosity.

5. "Instantaneous addition of a load" implies one or more large mass waste events that, if there are multiple, occurred within a time span geologically so short that they were not separated by regular sedimentation and were not individually influenced by tectonic shortening.

[12] The series of nine experiments includes test runs to determine the appropriate dimensions of the initial model and of the added sand layer that simulates the "instantaneous addition of a load." Results from test models revealed the need for long basal silicone layers so that their ends does not drive and localize thrusting at this experimentally implemented tip. Test experiments that included erosion in the source area of the "mass waste event" show little variation in wedge evolution as a function of the amount of erosion. Therefore, the presented experiments concentrate on the frontal wedge covered by the load, studying the effects of different amounts of added load.

[13] Brittle, i.e., frictional, layers are made up of pure eolean quartz sand (mean density ~1500 kg m^{-3}, negligible cohesion and a coefficient of internal friction ~0.58). Colored sand layers visualize internal deformation in the brittle

layers. Classical methods were unable to define the rheology of overpressured shales because of their high water content. Overpressured rocks have been approximately simulated in analog experiments (1) by injecting compressed air into sand packs [e.g., *Mourgues and Cobbold*, 2006], (2) as a ductile elastoplastic, nonviscous material using oil-water emulsions [e.g., *Verschuren et al.*, 1996], or (3) as a Newtonian viscous fluid [e.g., *Morency et al.*, 2007]. Being left with large uncertainties and following other experimentalists [e.g., *Bonini*, 2001; *Costa and Vendeville*, 2002; *Fort et al.*, 2004], we employed very weak (viscosity $\mu = 2.4 \times 10^4$ Pa s at laboratory temperature) Newtonian viscous silicone putty as analog to overpressured layers. Indeed, experimental results are discussed in the light of first-order stress distribution and shear stress contrast between adjacent layers [e.g., *Davy and Cobbold*, 1991; *Brun*, 1999], leaving aside the question of exact rheological properties of natural samples and, therefore, that of the strict rheological similarity between prototype and model.

[14] The models used in this work initially consisted of a sand stratum resting on a ductile basal silicone putty sheet (Table 1 and Figure 5). The modeling apparatus used for experiments 1–3 consisted of a 250 × 40 cm rigid table with lateral glass walls and a base that was slightly inclined toward the vertical backstop (Figure 5a). The backstop advanced at constant velocity to shorten the models, including their basal silicone layer. In experiment 4, the basal plastic sheet was pulled underneath the backstop instead of advancing the vertical backstop as in the other experiments (Figure 5b). In order to reduce the boundary effects inherent to rigid vertical walls, notably vertical shear, a small extra charge was added in front of the backstop. The emplacement of a mass flow was introduced by "instantaneously" adding a wedge-shaped sand layer during ongoing shortening. This added layer, or load, thinned out frontward and covered the previously developed thrust wedge and parts of the adjacent undeformed, model "foreland" (Figure 5). The silicone layer was at least 20 cm longer than the area covered by the added sand "mass flow" to avoid interference. Shortening was continued (phase 2 in the discussion) to observe potential changes in deformation style and pattern. We did not apply any sedimentation/erosion. Sections cut after shortening were used to support observations and to illustrate the discussion.

2.2. Results

[15] The preload wedge formation (phase 1) is similar to purely frictional wedges containing ductile décollements in
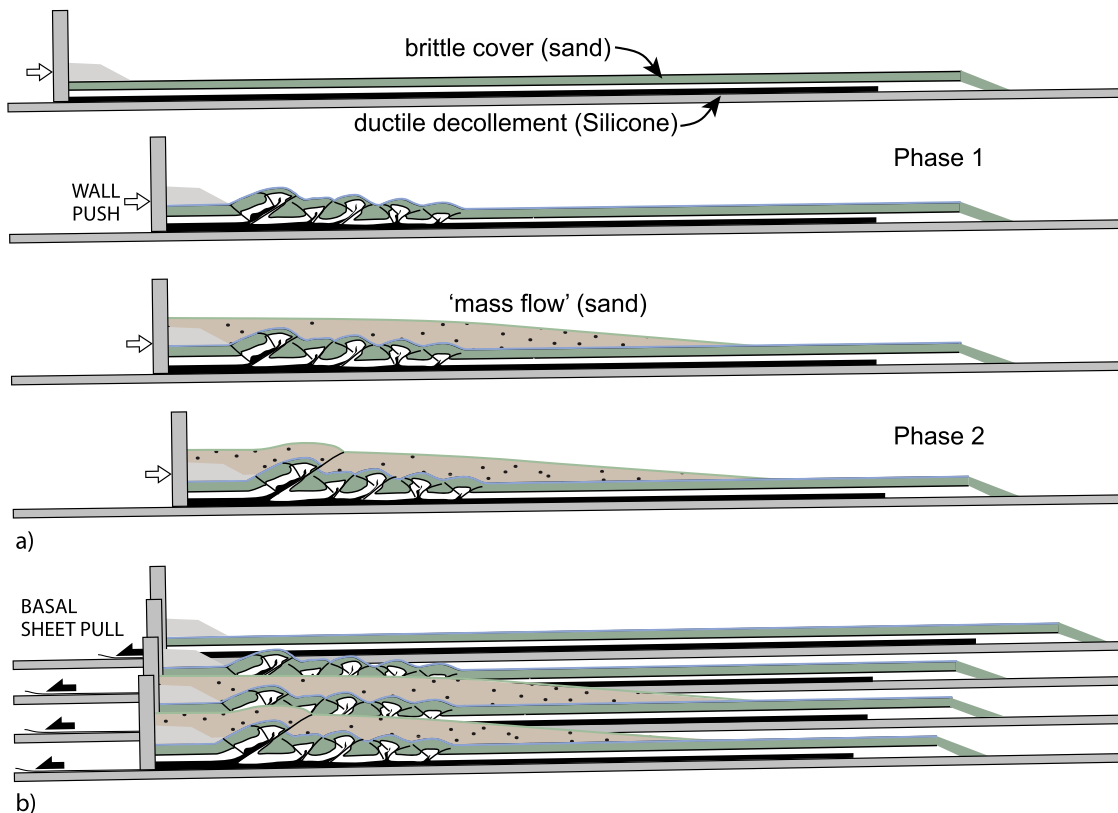
Figure 5. Experimental setups. (a) In models 1–3, shortening is obtained by pushing the backstop. In phase 1, a thrust wedge is formed by shortening of the brittle sand layer laid on a ductile silicone putty sheet. In phase 2, shortening continues at the same rate as during phase 1 after "instantaneous" emplacement of an extra sand load that covers the thrust wedge beyond its frontal thrust. (b) In model 4, shortening is due to pulling a thin plastic sheet below the sand-silicone model, while the backstop is fixed. Other characteristics are as in models 1–3.

terms of movement direction, spacing of thrust faults and in- and out-of-sequence faulting [*Costa and Vendeville*, 2002; *Smit et al.*, 2003]. The basal décollement favors coeval activity along several thrusts. The amount of shortening needed to form a wedge with a stable surface slope depends on the efficacy of the basal décollement [*Smit et al.*, 2003]. The efficacy itself is dependant on the shear-stress ratio between brittle cover (B) and ductile décollement (D) and increases with increasing B/D stress ratio. Initial conditions favor in-sequence, forward propagation with a maximum spacing of few centimeters between the main, emerging thrust ramps in all models.

[16] Model 1 represents a wedge to which a small load was added and model 2 represents one on which a thick load was laid over the thrust wedge; a load of intermediate thickness was sprayed over the wedge of models 3 and 4. Addition of the load decreased the surface dip angle in all models (Table 1).

[17] In model 1 a thrust wedge of three in-sequence thrust units is formed during phase 1 (Figure 6a). After addition of a thin and short load, thrusts 2 and especially 3 remain active during phase 2 (Figure 6b). Frontward propagation occurs by the formation of a new thrust unit, thrust 4,

immediately in front of the still active thrust 3 (Figure 6c). In short, the wedge continued growing without consequential changes in the thrusting pattern.

[18] Covering model 2 with a thick and long load (Figure 7b) stopped displacement along existing thrust planes 1–6. Further shortening was accommodated along newly formed thrusts, thrusts 7 and 8, at the front of the added load. These new thrust propagated in-sequence forward, forming a new thrust wedge in front of the load (Figure 7c). The loaded area did not display additional deformation until the preload thrust 5 was reactivated out of sequence.

[19] At the end of phase 1 of model 3, a shorter thrust wedge than in model 2, with four well-developed thrust units was formed (Figure 8). After addition of a sand load of intermediate thickness, thrusts 3 and 4 remained active, affecting the new load cover. Besides continued activity of these old thrusts, two new thrust units, thrusts 6 and 7, formed at the front of the added sand.

[20] Model 4 (Figures 9) shows a deformation pattern comparable to that of model 3 (Figure 8). Deformation jumps to the front of the added sand in the beginning of phase 2 with the formation of new thrusts 5 and 6. Old thrust 1 is slightly reactivated (Figure 9b). Further shortening continued
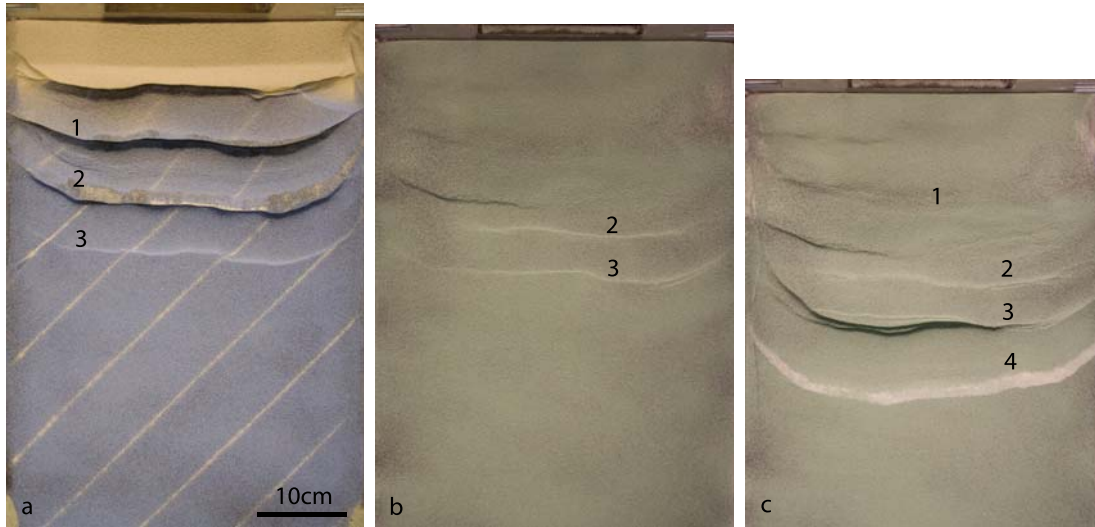
Figure 6. Surface views of model 1, numbers designates thrusts in order of appearance (parameters in Table 1). (a) At end of phase 1 after 7.5 cm shortening, three in-sequence thrusts constitute a thrust wedge. (b) In early phase 2, first structures after addition of a relatively thin sand load (green surface), thrusts 2 and, especially, 3 remained active. (c) After 5 cm shortening during phase 2, there is frontward propagation with the formation of a new thrust unit 4 in front of the still active thrust 3.

activity of thrusts 5 and 6 at the front of the added layer while thrusts 1 and 3 were clearly reactivated (Figures 9 and 10).

3. Discussion

3.1. Wedge Equilibrium

[21] The critical taper theory professes how a decrease in surface slope may compel reactivation of existing thrusts to thicken the wedge. *Morley* [2007] argued that deposition of an olistostrome diminishes the slope of the tapered wedge and therefore triggers a change in deformation. In each of the presented experiments the average surface slope became smaller with addition of the extra sand. The internal wedge of model 1 continued to thicken through movement along existing thrusts. Thickening of models 2 and 3 after load addition was preceded and then accompanied by thrusting
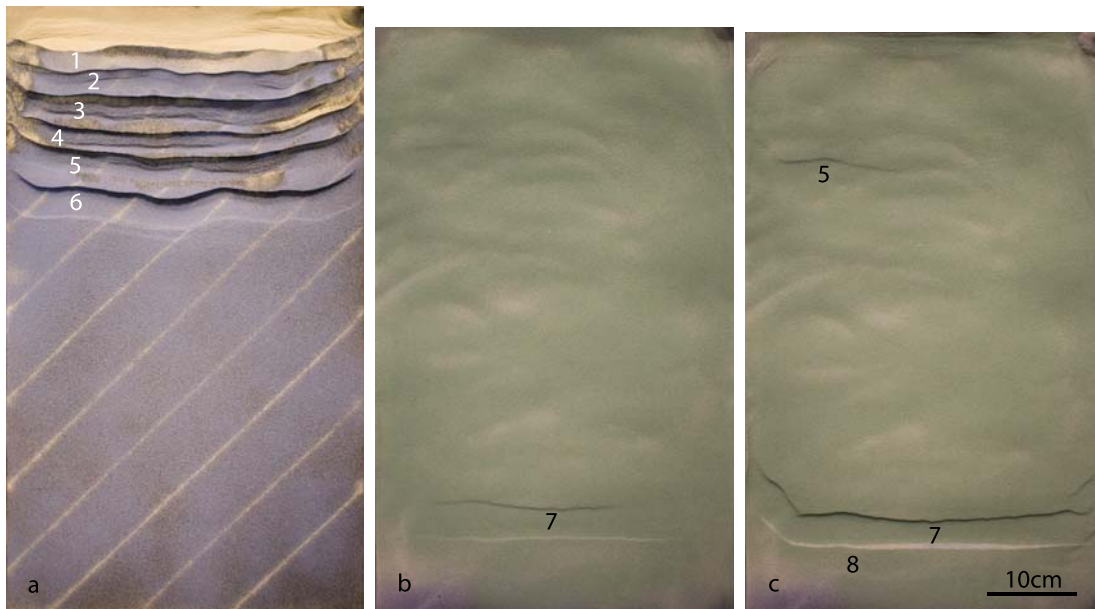

Figure 7. Surface views of model 2 (parameters in Table 1). (a) At end of phase 1 the thrust wedge is made of six thrust units. (b) In early phase 2, thrust 7 is the first structure rupturing the surface at the front of the relatively thick sand load (green surface). (c) At end of phase 2, thrust 8 occurred in front of thrust 7. Out-of-sequence reactivation of thrust 5 occurred after the formation of thrust 8.
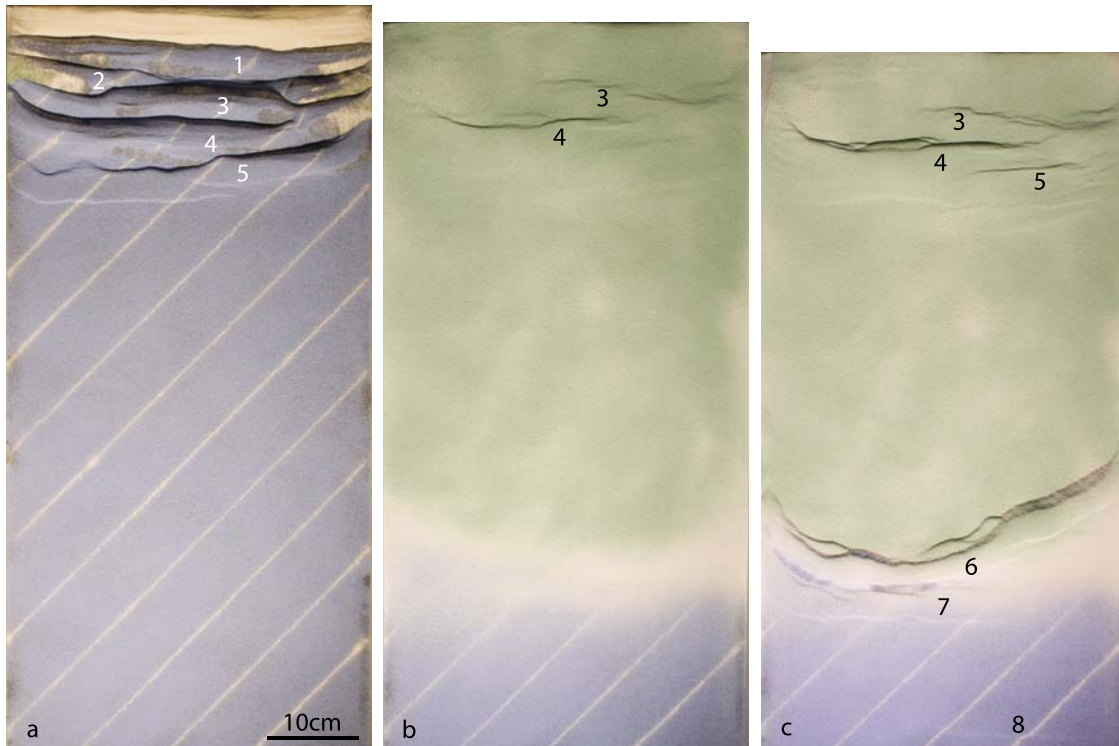
Figure 8. Surface views of model 3 (parameters in Table 1). (a) At end of phase 1, a thrust wedge forms with four thrust units while thrust 5 is being formed. (b) In early phase 2, thrusts 3 and 4 remain active after addition of the intermediate thickness sand load (green surface). (c) At end of phase 2, besides activity of old thrusts at the back of the system, two new thrust units, thrusts 6 and 7, have formed at the tip of the added sand. Thrust 8 appeared just before shortening was stopped and marks the end of the basal ductile layer.

ahead of the added load, thus indicating that the covered wedges had reached their states of critical taper.

[22] In the application of the critical taper theory to wedges on a ductile décollement, the décollement is introduced in the analytical solution by zero basal friction [e.g., *Davis and Engelder*, 1985; *Dahlen*, 1990]. It follows that thrust wedges on a basal ductile décollement can reach equilibrium at very low (≤1°) critical taper but this analytical solution explains or predicts neither temporal changes within a wedge nor the observed differences between wedges.

[23] The resistance to shear in a ductile layer like salt or overpressured shale may be 2 orders of magnitude weaker than that of the brittle overburden, but it increases with decreasing thickness of the ductile layer; this is due to the strain rate dependency of viscosity. Because the maximum shear stress in a brittle layer and the shear stresses in a ductile layer depend in opposite ways on layer thickness, the stress ratio of brittle to ductile layer varies strongly from back to toe in wedge shaped systems [e.g., *Smit et al.*, 2003]. Such systems cannot be described only by a brittle wedge whose basal resistance is zero.

[24] Previous experimental studies have analyzed the effects of brittle-ductile coupling in terms of relative strength between the brittle and ductile layers in both extensional [*Nalpas and Brun*, 1993; *Brun*, 1999, 2002] and compression settings [*Bonini*, 2001; *Smit et al.*, 2003]. This approach allows taking into account lateral variations in rheology and geometry of separate layers. It consists in considering the geometry and boundary conditions of the thrust wedge and assuming constant strain rates throughout the wedge. The velocity at the brittle-ductile interface, i.e., at the site of thrust initiation, is taken to be equal to the backstop velocity. Since the mass waste event does not change the properties and geometry of the ductile layer, we focus our stress analysis on the changing geometry of the brittle layer. However, the role of the weak ductile décollement is vital in that it favors deformation mobility, i.e., the possibility for deformation to shift to different parts of the wedge.

[25] The vertical normal stress σ in the brittle layer is given by

$$\sigma = \rho g T_b, \qquad (1)$$

where ρ is the sand density, g the gravity acceleration, and T_b the thickness of the sand layer. Because $\sigma = \sigma_3$ in compression, the maximum differential stress is

$$\sigma_1 - \sigma_3 = 2\rho g T_b. \qquad (2)$$

Consequently, the maximum differential stress in the brittle layer only depends on layer thickness for a given density (ρ). A thrust remains active as long as the stresses needed to
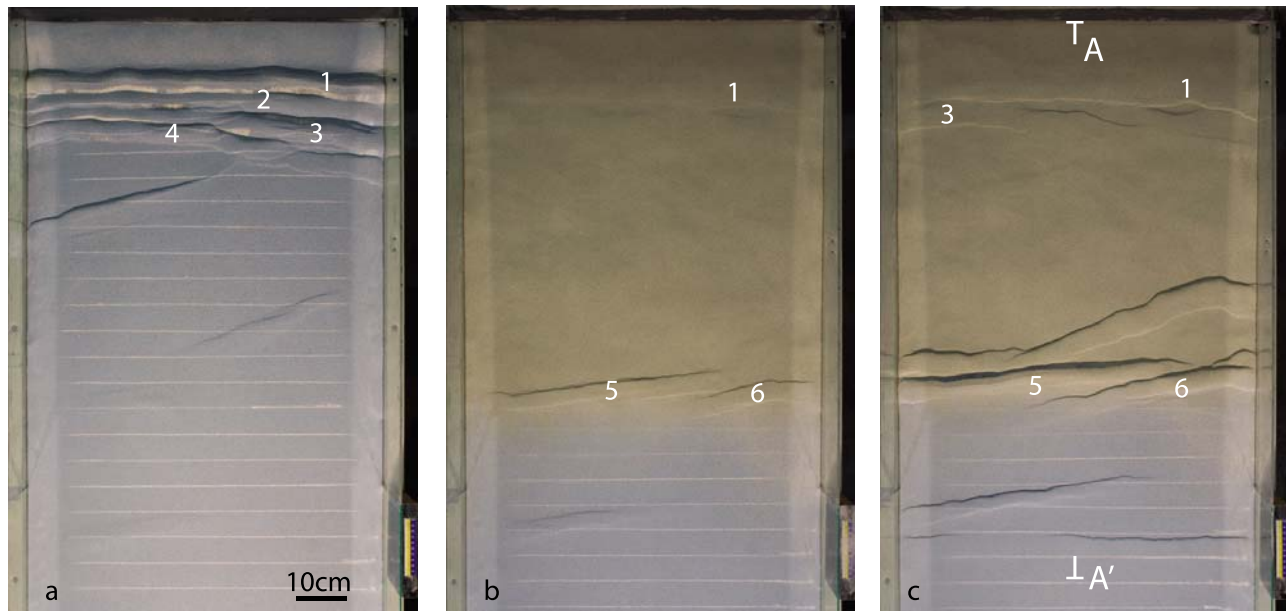
Figure 9. Surface views of model 4, with deformation generated by pulling the base underneath the backstop (Figure 5b). See Figure 10 for cross section AA′. (a) Phase 1 thrust wedge. Oblique, numberless structures are likely caused by folds in the pulled plastic sheet at the base of the model; they do not interfere with the main wedge development. (b) In early phase 2, deformation jumped nearly immediately to the front of the added sand load of intermediate thickness with the formation of thrusts 5 and 6. Thrust 1 is slightly reactivated. (c) At end of phase 2, there is continued activity at the front of the added load while thrusts 1 and 3 are reactivated.

overcome friction are smaller than the stresses needed to switch displacement to another existing thrust or to generate a new one. Unloading in the source area of a mass waste event decreases the strength of the brittle wedge and, therefore, the differential stress required for thrusting, proportionally to the amount of material removed (Figure 11a). A decrease of normal stress on existing thrust planes in this area favors reactivation. The effects in the loaded area of redeposition are more diverse. The surface of the unlithified mass flow takes a flatter slope than that of the generally lithified, Coulomb wedge. Where thrust units already exist, the sudden load on the already thickened wedge remains thin for simple geometrical reasons and contributes little to the local wedge (Figure 11b). The preload thrust planes remain weak zones that may be reactivated more easily than new thrusts are created in this area. For the same reasons, the load is thickest at the preload thrust front and its relative contribution to the local wedge thickness is largest. This zone is particularly resistant to deformation due to the lack of inherited and weak thrust planes. The load thins toward its frontal tip where the total thickness of the brittle layer is smallest and is a favorable location for new thrusts due to stress propagation through the basal ductile layer.

[26] Depending on the load length and thickness relative to the size of the preload thrust wedge, different scenarios for the thrust sequence after load emplacement are possible. The unloaded internal section will be the location for wedge thickening by fault reactivation and possibly backthrusting in all scenarios.

3.2. Application to Makran

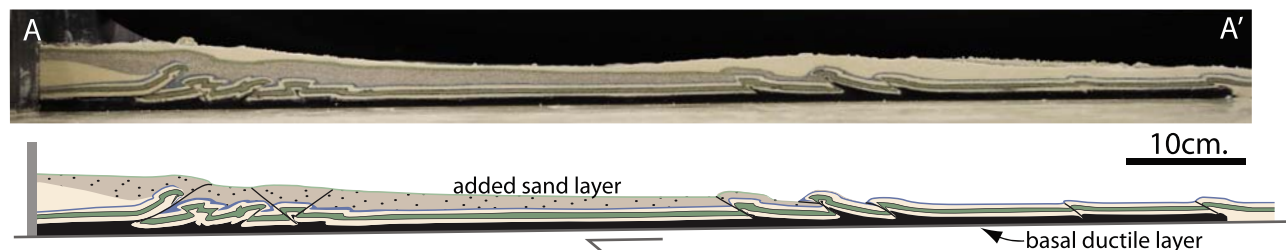[27] For the modeling results to be relevant to the Makran accretionary wedge, the assumptions on which the experi-

Figure 10. Photo and sketch of cross section AA′ through model 4 (Figure 9 for location). Only faults that are active during phase 2 are drawn.
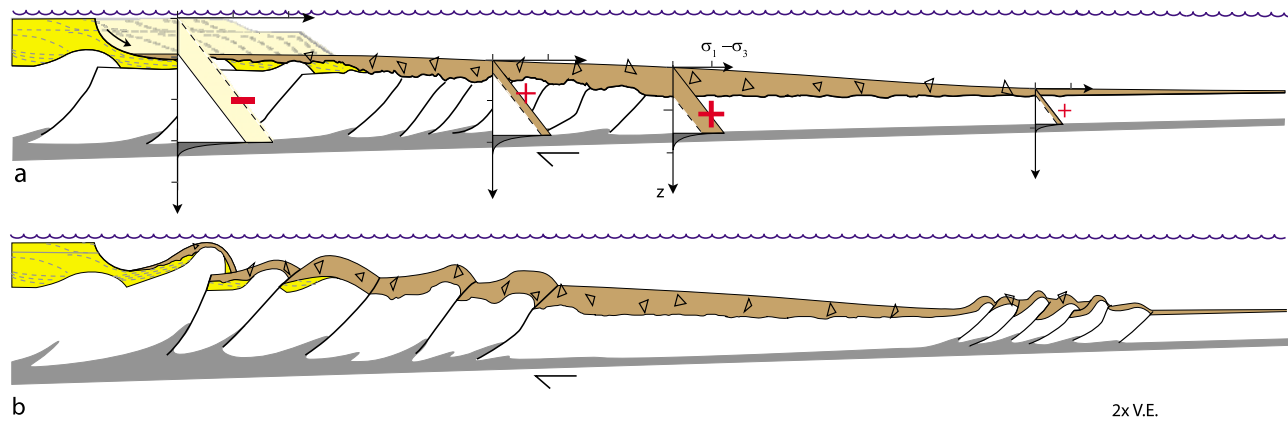
Figure 11. Schematic profile of an accretionary wedge before (Figure 11a) and just after (Figure 11b) olistostrome emplacement (continuation of Figure 4). (a) Strength profiles indicate the strength distribution in the wedge before and after olistostrome emplacement. The pale yellow in strength profile 1 illustrates the weakening of the source area of the mass waste event, and the brown in strength profiles 2–4 illustrates the local strengthening due to the added load (olistostrome). (b) Continued shortening is concentrated along a few of the preolistostrome faults causing rapid uplift and erosion of the old wedge. Part of the shortening is simultaneously transferred to the front of the olistostrome where new thrusts form, bypassing the thick part of the olistostrome in front of the existing thrust wedge.

ments were designed must apply to the Makran as well. The presence of weak décollements is vital. Several geological features strongly support the existence of one or more décollement levels. The rocks cropping out in the Makran wedge have not been subjected to deep regional metamorphism inherent to thrust-related burial. This implies that the exposed rock units have stayed in the shallow levels of the upper crust and that the growth of the wedge has occurred deeper, by tectonic accretion below a décollement surface. In addition, mud volcanoes along the coast point to the existence of fluid-overpressured layers at depth. The absence of deep exhumation south of the ophiolitic zone, the large spacing between thrusts and the large width and low cross-sectional taper are other indirect arguments consistent with the presence of one or more weak décollements.

[28] Models 1 and 2 are not comparable to the geological interpretation of the Makran wedge; in model 1, the effects of the added load are so inconsequential that no effect on the deformation pattern and evolution were noticed (Figure 6); in model 2 the thick load locks the existing structures and further shortening is accommodated by new thrusts at the front of the load (Figure 7). Models 3 and 4 (Figures 8–10), however, compare to structural features of the Makran wedge (Figure 2b). In both the experiments and the Makran we observe two wedges (1) the preload, internal wedge and (2) the postload external wedge. Both wedges are separated by an undeformed or very weakly deformed zone covered by the load. In the Makran, this zone is fittingly characterized by very gentle folding. The observed segmentation, two wedges separated by a largely undeformed zone, can only take place in the presence of one or more weak décollements. Mud volcanism and seismic profiles [e.g., *Harms et al.*, 1984; *von Rad et al.*, 2000; *Delisle et al.*, 2002; *Grando*

and McClay, 2007; *Ellouz-Zimmermann et al.*, 2007b] indicate the presence of such décollement(s) in the offshore Makran.

[29] In models 3 and 4 the frontward shift of thrusting is almost immediate after load emplacement. The onset of shortening in the present-day offshore Makran is considered to be late Miocene, i.e., contemporaneous with, or shortly after emplacement of the widespread Tortonian olistostrome.

[30] Finally, postolistostrome and limited thrust reactivation in the internal wedge fit field observation. Although the contribution of movement along these old structures to the total amount of shortening is difficult to estimate, it is clear that the frontal Makran wedge that measures ~100 km across strike accommodates an important part of it (most of the 200 km expected if subduction was steadily 2 cm/yr since then).

4. Conclusions

[31] Analogue experiments on the effects of a mass flow on the structural development and mechanics of accretionary wedges provide insight in the interpretation of the Makran example. They confirm that large olistostromes, which are deposited instantaneously in terms of geological timescale, may destabilize the wedge equilibrium and accordingly trigger changes in the deformation patterns in the wedge area. This pattern depends on the relative size and extent of the olistostrome with respect to the earlier wedge it is deposited upon. When the olistostrome is too small, deformation will continue as is. The olistostrome will block activity of the old structures when it is relatively voluminous. A new thrust wedge will develop in front of the olistostrome, while the old thrust wedge and olistostrome-

covered part will largely escape further shortening. In the intermediate case, shortening will be contemporaneously accommodated along a number of old thrusts and in a new wedge in front of the mass flow. According to the latter scenario, the observed change in deformation style in the Makran from intense folding and thrusting to gentle folding and eventually a jump toward the present day, offshore front can be, at least partially, explained by the mass redistribution caused by the late Miocene olistostrome.

References

Barrier, L., T. Nalpas, D. Gapais, J. N. Proust, A. Casas, and S. Bourquin (2002), Influence of syntectonic sedimentation on thrust geometry. Field examples from the Iberian Chain (Spain) and analogue modelling, *Sediment. Geol.*, *146*, 91–104, doi:10.1016/S0037-0738(01)00168-3.

Bayer, R., J. Chery, M. Tatar, P. Vernant, M. Abbassi, F. Masson, F. Nilforoushan, E. Doerflinger, V. Regard, and O. Bellier (2006), Active deformation in Zagros-Makran transition zone inferred from GPS measurements, *Geophys. J. Int.*, *165*, 373–381, doi:10.1111/j.1365-246X.2006.02879.x.

Bonini, M. (2001), Passive roof thrusting and foreland-ward fold propagation in scaled brittle-ductile physical models of thrust wedges, *J. Geophys. Res.*, *106*, 2291–2311, doi:10.1029/2000JB900310.

Bonini, M. (2006), Detachment folding-related Miocene submarine slope instability in the Romagna Apennines (Italy), *J. Geophys. Res.*, *111*, B01404, doi:10.1029/2004JB003552.

Bonnet, C., J. Malavieille, and J. Mosar (2007), Interactions between tectonics, erosion, and sedimentation during the recent evolution of the Alpine orogen: Analogue modeling insights, *Tectonics*, *26*, TC6016, doi:10.1029/2006TC002048.

Bonnet, C., J. Malavieille, and J. Mosar (2008), Surface processes versus kinematics of thrust belts: Impact on rates of erosion, sedimentation, and exhumation—Insights from analogue models, *Bull. Soc. Geol. Fr.*, *179*, 297–314, doi:10.2113/gssgfbull.179.3.297.

Brun, J.-P. (1999), Narrow rifts versus wide rifts: Inferences for the mechanics of rifting from laboratory experiments, *Philos. Trans. R. Soc. London*, *357*, 695–712, doi:10.1098/rsta.1999.0349.

Brun, J.-P. (2002), Deformation of the continental lithosphere: insights from brittle-ductile models, in *Deformation Mechanisms, Rheology and Tectonics: Current Status and Future Perspectives*, edited by S. De Meer et al., pp. 355–370, Geol. Soc., London.

Burg, J.-P., D. Bernoulli, J. Smit, A. Dolati, and A. Bahroudi (2008), A giant catastrophic mud-and-debris flow in the Miocene Makran, *Terra Nova*, *20*, 188–193, doi:10.1111/j.1365-3121.2008.00804.x.

Callot, P., T. Sempere, F. Odonne, and E. Robert (2008), Giant submarine collapse of a carbonate platform at the Turonian-Coniacian transition: The Ayabacas Formation, southern Peru, *Basin Res.*, *20*, 333–357, doi:10.1111/j.1365-2117.2008.00358.x.

Chapple, W. M. (1978), Mechanics of thin-skinned fold-and-thrust belts, *Geol. Soc. Am. Bull.*, *89*, 1189–1198, doi:10.1130/0016-7606(1978)89<1189:MOTFB>2.0.CO;2.

Costa, E., and B. C. Vendeville (2002), Experimental insights on the geometry and kinematics of fold-and-thrust belts above weak, viscous evaporitic decollement, *J. Struct. Geol.*, *24*, 1729–1739, doi:10.1016/S0191-8141(01)00169-9.

Dahlen, F. A. (1990), Critical taper model of fold-and-thrust belts and accretionary wedges, *Annu. Rev. Earth Planet. Sci.*, *18*, 55–99, doi:10.1146/annurev.ea.18.050190.000415.

Davis, D. M., and T. Engelder (1985), The role of salt in fold-and-thrust belts, *Tectonophysics*, *119*, 67–88, doi:10.1016/0040-1951(85)90033-2.

Davis, D., J. Suppe, and F. A. Dahlen (1983), Mechanics of fold-and-thrust belts and accretionary wedges, *J. Geophys. Res.*, *88*, 1153–1172, doi:10.1029/JB088iB02p01153.

Davy, P., and P. R. Cobbold (1991), Experiments on shortening of a 4-layer model of the continental lithosphere, *Tectonophysics*, *188*, 1–25, doi:10.1016/0040-1951(91)90311-F.

Delisle, G., U. von Rad, H. Andruleit, C. H. von Daniels, A. R. Tabrez, and A. Inam (2002), Active mud volcanoes on- and offshore eastern Makran, Pakistan, *Int. J. Earth Sci.*, *91*, 93–110, doi:10.1007/s005310100203.

Ellouz-Zimmermann, N., E. Deville, C. Müller, S. Lallemant, A. B. Subhani, and A. R. Tabreez (2007a), Impact of sedimentation on convergent margin tectonics: Example of the Makran accretionary prism (Pakistan), in *Thrust Belts and Foreland Basins: From Fold Kinematics to Hydrocarbon Systems*, edited by O. L. Lacombe et al., pp. 326–348, Springer, Berlin.

Ellouz-Zimmermann, N., et al. (2007b), Offshore frontal part of the Makran accretionary prism (Pakistan) the Chamak Survey, in *Thrust Belts and Foreland Basins: From Fold Kinematics to Hydrocarbon Systems*, edited by O. L. Lacombe et al., pp. 349–364, Springer, Berlin.

Fort, X., J. P. Brun, and F. Chauvel (2004), Salt tectonics on the Angolan Margin, syn-sedimentary deformation processes, *AAPG Bull.*, *88*, 1523–1544.

Gee, M. J. R., H. S. Uy, J. Warren, C. K. Morley, and J. J. Lambiase (2007), The Brunei slide: A giant submarine landslide on the North West Borneo Margin revealed by 3D seismic data, *Mar. Geol.*, *246*, 9–23, doi:10.1016/j.margeo.2007.07.009.

Grando, G., and K. McClay (2007), Morphotectonics domains and structural styles in the Makran accretionary prism, offshore Iran, *Sediment. Geol.*, *196*, 157–179, doi:10.1016/j.sedgeo.2006.05.030.

Graveleau, F., and S. Dominguez (2008), Analogue modelling of the interaction between tectonics, erosion and sedimentation in foreland thrust belts, *C. R. Geosci.*, *340*, 324–333, doi:10.1016/j.crte.2008.01.005.

Harms, J. C., H. N. Cappel, and D. C. Francis (1984), The Makran Coast of Pakistan; its stratigraphy and hydrocarbon potential, in *Marine Geology and Oceanography of Arabian Sea and Coastal Pakistan*, edited by U. Haq Bilal and D. Milliman John, pp. 3–26, Van Nostrand Reinhold, New York.

Harrison, J. V. (1944), Mud volcanoes on the Makran coast, *Geogr. J.*, *103*, 180–181.

Hubbert, M. K. (1937), Theory of scale models as applied to the study of geologic structures, *Geol. Soc. Am. Bull.*, *48*, 1459–1519.

Konstantinovskaia, E., and J. Malavieille (2005), Erosion and exhumation in accretionary orogens: Experimental and geological approaches, *Geochem. Geophys. Geosyst.*, *6*, Q02006, doi:10.1029/2004GC000794.

Leturmy, P., J. L. Mugnier, P. Vinour, P. Baby, B. Colletta, and E. Chabron (2000), Piggyback basin development above a thin-skinned thrust belt with two detachment levels as a function of interactions between tectonic and superficial mass transfer: the case of the Subandean Zone (Bolivia), *Tectonophysics*, *320*, 45–67, doi:10.1016/S0040-1951(00)00023-8.

Lucente, C. C., and G. A. Pini (2008), Basin-wide mass-wasting complexes as markers of the Oligo-Miocene foredeep-accretionary wedge evolution in the northern Apennines, Italy, *Basin Res.*, *20*, 49–71, doi:10.1111/j.1365-2117.2007.00344.x.

McCall, G. J. H. (2002), A summary of the geology of the Iranian Makran, in *The Tectonic and Climate Evolution of the Arabian Sea Region*, edited by P. D. Clift et al., *Geol. Soc. Spec. Publ.*, *195*, 147–204, doi:10.1144/GSL.SP.2002.195.01.10.

McCall, G. J. H., and R. G. W. Kidd (1982), The Makran, southeastern Iran: The anatomy of a convergent plate margin active from Cretaceous to present, in *Trench-Forearc Geology: Sedimentation and Tectonics on Modern and Ancient Active Plate Margins*, edited by J. K. Leggett, pp. 387–397, Geol. Soc., London.

Medialdea, T., R. Vegas, L. Somoza, J. T. Vazquez, A. Maldonado, V. Diaz-del-Rio, A. Maestro, D. Cordoba, and M. C. Fernandez-Puga (2004), Structure and evolution of the "olistostrome" complex of the Gibraltar Arc in the Gulf of Cádiz (eastern central Atlantic): Evidence from two long seismic cross-sections, *Mar. Geol.*, *209*, 173–198, doi:10.1016/j.margeo.2004.05.029.

Moore, D. G., J. R. Curray, and F. J. Emmel (1976), Large submarine slide (olistostrome) associated with Sunda Arc subduction zone, northeast Indian Ocean, *Mar. Geol.*, *21*, 211–226, doi:10.1016/0025-3227(76)90060-8.

Morency, C., R. S. Huismans, C. Beaumont, and P. Fullsack (2007), A numerical model for coupled fluid flow and matrix deformation with applications to disequilibrium compaction and delta stability, *J. Geophys. Res.*, *112*, B10407, doi:10.1029/2006JB004701.

Morley, C. K. (2007), Interaction between critical wedge geometry and sediment supply in a deep-water fold belt, *Geology*, *35*, 139–142, doi:10.1130/G22921A.1.

Mourgues, R., and P. R. Cobbold (2006), Thrust wedges and fluid overpressures: Sandbox models involving pore fluids, *J. Geophys. Res.*, *111*, B05404, doi:10.1029/2004JB003441.

Mugnier, J. L., P. Baby, B. Colletta, P. Vinour, P. Bale, and P. Leturmy (1997), Thrust geometry controlled by erosion and sedimentation; a view from analogue models, *Geology*, *25*, 427–430, doi:10.1130/0091-7613(1997)025<0427:TGCBEA>2.3.CO;2.

Nalpas, T., and J. P. Brun (1993), Salt flow and diapirism related to extension at crustal scale. New insights into salt tectonics, *Tectonophysics*, *228*, 349–362, doi:10.1016/0040-1951(93)90348-N.

Persson, K. S., D. Garcia-Castellanos, and D. Sokoutis (2004), River transport effects on compressional belts: First results from an integrated analogue-numerical model, *J. Geophys. Res.*, *109*, B01409, doi:10.1029/2002JB002274.

Pini, G. A. (1999), Tectonosomes and olistostromes in the argille scagliose of the northern Apennines, Italy, *Spec. Pap. Geol. Soc. Am.*, *335*, 70 pp.

Platt, J. P., J. K. Leggett, J. Young, H. Raza, and S. Alam (1985), Large-scale sediment underplating in the Makran accretionary prism, *Geology*, *13*, 507–511, doi:10.1130/0091-7613(1985)13<507:LSUITM>2.0.CO;2.

Smit, J. H. W., J. P. Brun, and D. Sokoutis (2003), Deformation of brittle-ductile thrust wedges in experiments and nature, *J. Geophys. Res.*, *108*(B10), 2480, doi:10.1029/2002JB002190.

Smith, W. H. F., and D. T. Sandwell (1997), Global sea-floor topography from satellite altimetry and ship depth soundings, *Science*, *277*, 1956–1962, doi:10.1126/science.277.5334.1956.

Snead, R. E. (1964), Active mud volcanoes of Baluchistan, west Pakistan, *Geogr. Rev.*, *54*, 546–560, doi:10.2307/212981.

Storti, F., and K. McClay (1995), Influence of syntectonic sedimentation on thrust wedges in analogue models, *Geology*, *23*, 999–1002, doi:10.1130/0091-7613(1995)023<0999:IOSSOT>2.3.CO;2.

Verschuren, M., D. Nieuwland, and J. Gast (1996), Multiple detachment levels in thrust tectonics: Sandbox experiments and palinspastic reconstruction, in *The Origin and Evolution of the Caribbean Plate*, edited by K. H. James, M. A. Lorente, and J. L. Pindell, *Geol. Soc. Spec. Publ.*, 99, 227–234, doi:10.1144/GSL.SP.1996.099.01.17.

Vigny, C., P. Huchon, J. Ruegg, K. Khanbari, and L. M. Asfaw (2006), Confirmation of Arabia plate slow motion by new GPS data in Yemen, *J. Geophys. Res.*, *111*, B02402, doi:10.1029/2004JB003229.

von Rad, U., et al. (2000), Gas and fluid venting at the Makran accretionary wedge off Pakistan, *Geo Mar. Lett.*, *20*, 10–19, doi:10.1007/s003670000033.

J.-P. Burg and A. Dolati, Geological Institute, ETH Zurich, Sonneggstrasse 5, CH-8092 Zürich, Switzerland.

J. Smit, ISTeP, UMR 7193, Université Pierre and Marie Curie, Case 129, 4, Place Jussieu, F-75252 Paris CEDEX 05, France. (jeroen.smit@upmc.fr)

D. Sokoutis, Netherlands Research Centre for Integrated Solid Earth Sciences, Faculty of Earth and Life Sciences, De Boelelaan 1085, Vrije Universiteit, NL-1081 HV Amsterdam, Netherlands.